

RESEARCH

Open Access



Super-resolution deep learning reconstruction at coronary computed tomography angiography to evaluate the coronary arteries and in-stent lumen: an initial experience

Makoto Orii^{1*}, Misato Sone¹, Takeshi Osaki¹, Yuta Ueyama², Takuya Chiba², Tadashi Sasaki² and Kunihiro Yoshioka¹

Abstract

A super-resolution deep learning reconstruction (SR-DLR) algorithm trained using data acquired on the ultrahigh spatial resolution computed tomography (UHRCT) has the potential to provide better image quality of coronary arteries on the whole-heart, single-rotation cardiac coverage on a 320-detector row CT scanner. However, the advantages of SR-DLR at coronary computed tomography angiography (CCTA) have not been fully investigated. The present study aimed to compare the image quality of the coronary arteries and in-stent lumen between SR-DLR and model-based iterative reconstruction (MBIR). We prospectively enrolled 70 patients (median age, 69 years; interquartile range [IQR], 59–75 years; 50 men) who underwent CCTA using a 320-detector row CT scanner between January and August 2022. The image noise in the ascending aorta, left atrium, and septal wall of the ventricle was measured, and the signal-to-noise ratio (SNR) and contrast-to-noise ratio (CNR) in the proximal coronary arteries were calculated. Of the twenty stents, stent strut thickness and luminal diameter were quantitatively evaluated. The image noise on SR-DLR was significantly lower than that on MBIR (median 22.1 HU; IQR, 19.3–24.9 HU vs. 27.4 HU; IQR, 24.2–31.2 HU, $p < 0.01$), whereas the SNR (median 16.3; IQR, 11.8–21.8 vs. 13.7; IQR, 9.9–18.4, $p = 0.01$) and CNR (median 24.4; IQR, 15.5–30.2 vs. 19.2; IQR, 14.1–23.2, $p < 0.01$) on SR-DLR were significantly higher than that on MBIR. Stent struts were significantly thinner (median, 0.68 mm; IQR, 0.61–0.78 mm vs. 0.81 mm; IQR, 0.72–0.96 mm, $p < 0.01$) and in-stent lumens were significantly larger (median, 1.84 mm; IQR, 1.65–2.26 mm vs. 1.52 mm; IQR, 1.28–2.25 mm, $p < 0.01$) on SR-DLR than on MBIR. Although further large-scale studies using invasive coronary angiography as the reference standard, comparative studies with UHRCT, and studies in more challenging population for CCTA are needed, this study's initial experience with SR-DLR would improve the utility of CCTA in daily clinical practice due to the better image quality of the coronary arteries and in-stent lumen at CCTA compared with conventional MBIR.

Keywords Coronary computed tomography angiography, Super-resolution deep learning reconstruction, Model-based iterative reconstruction, Signal-to-noise ratio, Contrast-to-noise ratio

*Correspondence:
Makoto Orii
kori931@gmail.com

¹Department of Radiology, Iwate Medical University, 2-1-1, Idaidori, Yahaba 028-3695, Japan

²Center for Radiological Science, Iwate Medical University, 2-1-1, Idaidori, Yahaba 028-3695, Japan



© The Author(s) 2023. **Open Access** This article is licensed under a Creative Commons Attribution 4.0 International License, which permits use, sharing, adaptation, distribution and reproduction in any medium or format, as long as you give appropriate credit to the original author(s) and the source, provide a link to the Creative Commons licence, and indicate if changes were made. The images or other third party material in this article are included in the article's Creative Commons licence, unless indicated otherwise in a credit line to the material. If material is not included in the article's Creative Commons licence and your intended use is not permitted by statutory regulation or exceeds the permitted use, you will need to obtain permission directly from the copyright holder. To view a copy of this licence, visit <http://creativecommons.org/licenses/by/4.0/>. The Creative Commons Public Domain Dedication waiver (<http://creativecommons.org/publicdomain/zero/1.0/>) applies to the data made available in this article, unless otherwise stated in a credit line to the data.

Introduction

Coronary computed tomography angiography (CCTA) is a robust noninvasive imaging technique with high spatial and temporal resolutions. Its diagnostic accuracy is high for the exclusion of coronary artery disease; however, some factors such as high image noise, insufficient vessel enhancement, and blooming- and beam-hardening artifacts may hamper the precise evaluation of vessel stenosis and in-stent lumen [1–3].

Recent CCTA developments with an ultrahigh spatial resolution computed tomography (UHRCT) of 0.25 mm \times 128 or 160-row detector and model-based iterative reconstruction (MBIR) have overcome the limitations of the current CT spatial resolution. Several studies have reported higher diagnostic accuracy to detect significant stenosis with severely elevated calcium scores and in-stent patency with a diameter of ≥ 2.5 mm; however, the use of UHRCT is limited for patients with higher heart rate and weight and those with arrhythmia [4–6].

Recently, a super-resolution deep learning reconstruction (SR-DLR) algorithm trained using data acquired on the commercially available UHRCT system is available for the whole-heart, single-rotation cardiac coverage on a 320-detector row CT scanner [7, 8]. Several studies have reported the noise-reducing effect, improvement of spatial resolution, and the sharpness of margins and plaque detectability of coronary artery in SR-DLR compared with conventional reconstruction techniques [9, 10]. However, no studies have reported data on the potential value of SR-DLR at CCTA in the clinical setting. Thus, this study aimed to compare the image quality of the coronary arteries and in-stent lumen during CCTA reconstructed using SR-DLR and MBIR.

Materials and methods

Study population and design

Seventy consecutive patients who underwent CCTA for suspected or known coronary artery disease between January and August 2022 were prospectively enrolled at Iwate Medical University Hospital. Our exclusion criteria were renal insufficiency (estimated glomerular filtration rate < 30 mL/min per 1.73 m²), contrast agent allergy, history of bypass grafting, and potential pregnancy. Written informed consent was obtained from all participants, as approved by the institution's human research committee.

CT scanning

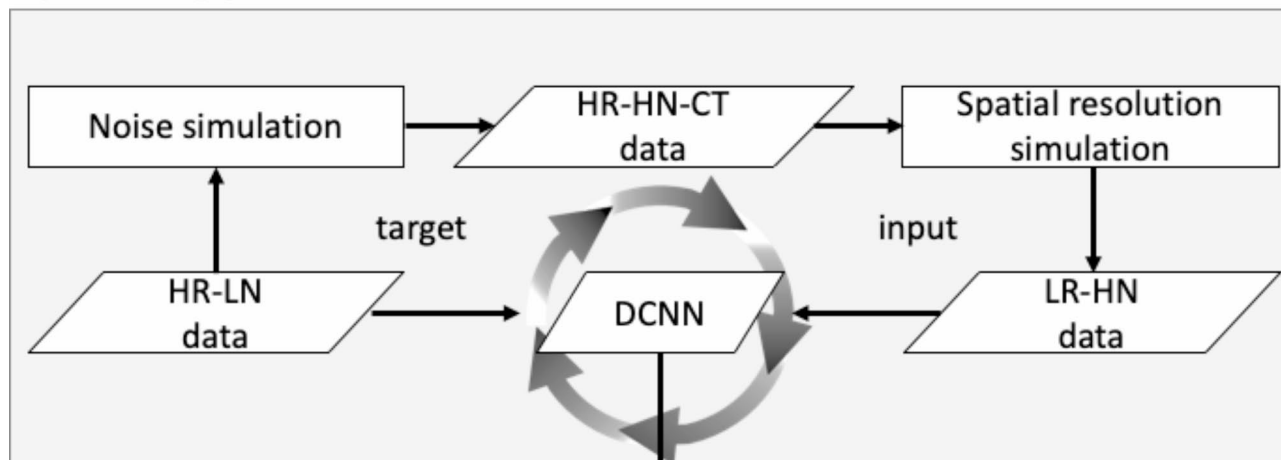
CT scans were performed using a 320-detector row CT scanner (Aquilion ONE PRISM Edition, Canon Medical Systems, Otawara, Japan). All patients were administered nitroglycerin. Patients with a heart rate of 65 bpm were administered oral beta-blockers 60 min before the CCTA scan based on the Society of Cardiovascular Computed Tomography guidelines [11, 12].

Coronary calcium scoring was performed using a prospective electrocardiogram (ECG) gating axial scan at a 75% RR interval, with 120 kV tube voltage and a 300-mA tube current. We delivered 25.9 mgI/kg/s of non-ionic contrast material (iopamidol [Iopamiron 370, Bayer, Osaka, Japan]) at a 10-s fixed duration, followed by a 35-mL saline flush administered using a 20-G intravenous catheter. The scan parameters were collimation of 320 \times 0.5 mm; rotation time, 0.275 s; z-coverage, 120–160 mm; tube voltage, 100 or 120 kV; and tube current, 180–750 mA. Prospective ECG gating scan with an acquisition window of 35–80% or 65–80% of the RR interval was used for patients with a heart rate of > 65 or ≤ 65 bpm, respectively. Retrospective ECG gating scan was used for patients with arrhythmia or those who could not sufficiently hold their breath. Experienced cardiovascular CT technologists determined the optimal stationary cardiac phase with minimum motion-free datasets. The dose length product was recorded for each participant, and the corresponding effective radiation dose was calculated using a standard conversion factor of 0.014 mSv/mGy cm for chest CT [13]. Axial images were reconstructed with 0.5-mm slice thickness and reconstruction interval. The image reconstruction field of view and the matrix size were 160–200 mm and 512 \times 512, respectively. All images were reconstructed using the SR-DLR (PIQE) and MBIR algorithm (FIRST, Canon Medical Systems Corp.).

Super-resolution deep learning reconstruction

Super resolution technology aims at restoring high resolution information from low or normal resolution inputs. SR-DLR archived not only high spatial resolution but also noise reduction [8, 14]. SR-DLR uses deep learning technology. Figure 1 shows the SR-DLR processing flow. In training process (a), the deep convolutional neural network (DCNN) is trained by a lot of target and input pairs. The high resolution and low noise data which are acquired on UHRCT scanner is used as target. UHRCT equipped with a finer size detector and smaller x-ray focal spot source, provides diagnostic images with two times the spatial resolution compared to 320-detector row CT scanner. “Noise simulation” to simulate low-exposure scan and “Spatial resolution simulation” to simulate spatial resolution degradation are applied to the target data, and low-quality data with low spatial resolution and high noise content are used as input data. By learning these pairs of target and input data, DCNN can learn both the generation model of spatial resolution recovery and the noise model. In reconstruction process (b), by using the pre-trained DCNN, SR-DLR can reconstruct the image with high spatial resolution and low noise from low spatial resolution and high noise on 320-detector row CT scanner.

a) Training process



b) Reconstruction process

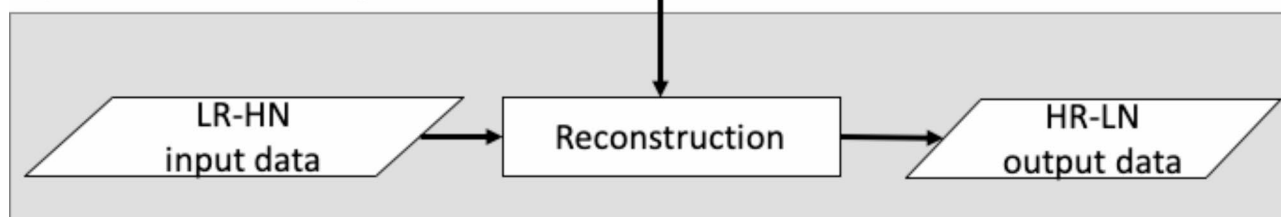


Fig. 1 Training and reconstruction processing flow of super-resolution deep learning reconstruction. In training process (a), the DCNN is trained by a lot of target and input pairs. The HR and LN data which are acquired on UHRCT scanner is used as target. The LR and HN data which is simulated from target is used as input. In reconstruction process (b), the LR and HN data is reconstructed using the trained DCNN. Then the HR and LN data is obtained. DCNN, deep convolutional neural network; HR, high resolution; LN, low noise; UHRCT, ultrahigh spatial resolution computed tomography; LR, low resolution; HN, high noise

Image interpretation

The image datasets were transferred to an off-line workstation, processed using commercially available software (Ziostation2, Ziosoft Inc., Tokyo, Japan) and two radiologists (M.O. and K.Y.) with 5 and 25 years of experience, respectively, in cardiovascular imaging performed all measurements. The readers were blinded to the clinical information and reconstruction method. In case of data analysis disagreed, a final decision was reached by consensus. The degree of coronary stenosis was graded as minimal (<25%), mild (25–49%), moderate (50–69%), and severe (70–99%) [15].

The overall image quality of each coronary artery segment was rated based on a four-point rating score for each coronary artery segment (4, excellent [minimal or no noise-related blurring and diagnostic information sufficient]; 3, good [some noise-related blurring and diagnostic information acceptable]; 2, fair [marked noise-related blurring and diagnostic information limited]; and 1, poor [blurry and diagnostic information impaired]) [16].

For SR-DLR and MBIR images, the image noise was recorded as the standard deviation (SD) of the

attenuation value in a circular region of interest (ROI) placed in the ascending aorta, left atrium, and septal wall of the ventricle. Then, signal-to-noise ratio (SNR) was calculated as signal/noise in the proximal right coronary artery and left main trunk [6]. The contrast-to-noise ratio (CNR) was calculated as follows: (mean vessel lumen signal–mean perivascular fat signal)/image noise in the ascending aorta [17, 18]. ROI measurements were performed by two radiologists on axial images, carefully preventing calcifications, plaques, and stenosis.

In-stent lumen assessability and quantitative stent analysis

Stents were considered assessable with the absence of partial volume effects by stent struts, beam hardening, motion artifacts, calcification, or low CNR and when the lumen within the stent was clearly visible [4, 19]. Figure 2 shows the calculation methods of lumen visibility measurements using the average attenuation profile in the axial plane [4, 19]. First, the stent proximal and distal edges on the curved planar reformation (CPR) image were determined, with the first, second, and third quartiles as calculated points. Second, after determining the center of the stent on the cross-sectional image (Fig. 2a

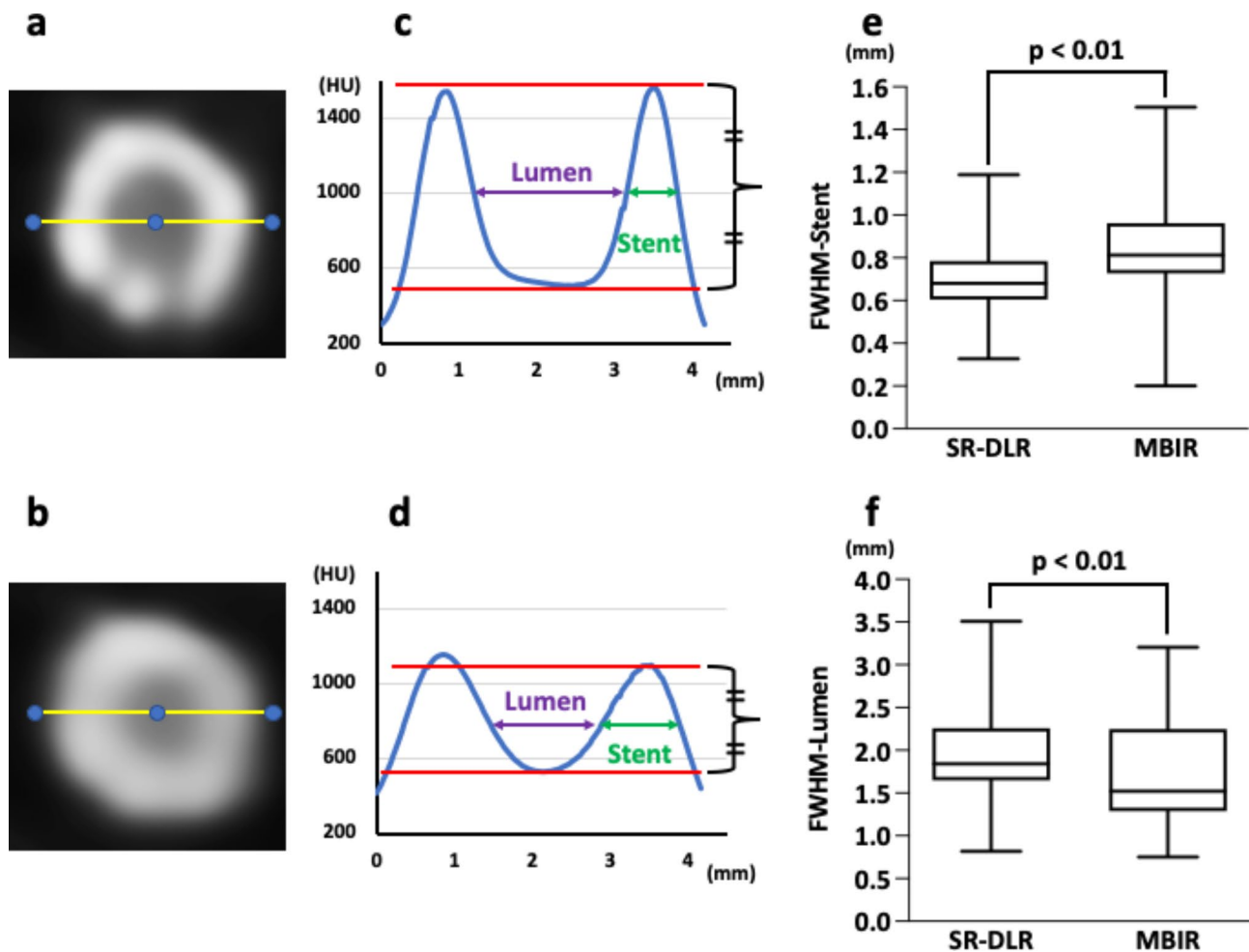


Fig. 2 Quantitative analysis of the lumen and stent in the coronary artery. After identifying the center of the stent on a cross-sectional image, attenuation profiles were calculated (a: SR-DLR, b: MBIR). FWHM-lumen and FWHM-stent were measured (c: SR-DLR, d: MBIR). FWHM-stent was significantly thinner ($p < 0.01$), whereas FWHM-lumen was significantly larger on SR-DLR ($p < 0.01$) than on MBIR (e, f). SR-DLR, super-resolution deep learning reconstruction; MBIR, model-based iterative reconstruction; FWHM-lumen, full width at half maximum of the lumen; FWHM-stent, full width at half maximum of the stent

and b), attenuation profiles were calculated, and the full width at half maximum of the lumen (FWHM-lumen) and full width at half maximum of the strut (FWHM-stent) were measured (Fig. 2c and d).

Invasive coronary angiography

Of the 70 patients, 14 underwent invasive coronary angiography. Experienced cardiovascular physicians performed selective invasive coronary angiography scanning using the standard Judkins technique, with a radial approach on a biplane angiography system (AlluraClarity FD10/10, Philips Electronics Japan, Tokyo Japan). Contrast medium was administered using an automated injection system (ACIST Cvi, ACIST Japan, Tokyo, Japan). The injection volume of contrast medium was 6.2 ml for the left coronary angiography, and 5.4 ml for the right coronary angiography.

Statistical analysis

Statistical analyses were performed using IBM® SPSS® 28.0.1 (IBM Corporation., Armonk, NY, USA). Continuous measurements are expressed as mean \pm SD for normally distributed variables or median (interquartile range [IQR], 25th–75th percentile) for nonparametric data and compared using Student's t-test or Mann–Whitney U-test as appropriate. Categorical variables are expressed as numbers and percentages. p-value of < 0.05 was considered statistically significant. The interobserver agreement between two radiologists regarding the qualitative evaluation was evaluated using the Cohen kappa κ coefficient. A κ value of more than 0.81 corresponded to excellent interobserver agreement, while values of 0.61–0.80 corresponded to good agreement.

Table 1 Baseline characteristics

Patient demographics (n = 70)	
Age, years	69 (59–75)
Male patients, n (%)	50 (71)
Height, cm	166 (159–171)
Weight, kg	65 (56–73)
Body surface area, m ²	1.7 (1.6–1.9)
Body mass index, kg/m ²	24 (22–26)
Hypertension, n (%)	48 (69)
Dyslipidemia, n (%)	39 (56)
Diabetes, n (%)	22 (31)
Smoking history (former or current), n (%)	18 (25)
Sinus rhythm, n (%)	65 (93)
Characteristics of CCTA scanning	
Mean heart rate during CCTA scanning, bpm	55 (51–61)
Tube voltage 100/120 kV, n (%)	32 (45)/38 (55)
Tube current	
With 100 kV, mA	315 (250–368)
With 120 kV, mA	400 (260–565)
Total dose length product, mGy*cm	62 (44–117)
Total effective radiation dose, mSv	0.9 (0.6–1.6)
Contrast medium dose, mL	48 (42–58)
Calcium score	16 (0–180)

CCTA, coronary computed tomography angiography

Table 2 Comparison of reconstruction time, image noise, signal-to-noise ratio, contrast-to-noise ratio, and visual evaluation of coronary arteries between super-resolution deep learning reconstruction and model-based iterative reconstruction

Parameter	SR-DLR	MBIR	p-value
Reconstruction time, s	97 (88–109)	173 (164–187)	< 0.01
Image noise, HU			
Ascending aorta	22.5 (20.5–31.8)	29.1 (26.2–36.6)	< 0.01
Left atrium	22.4 ± 4.0	30.1 ± 5.4	< 0.01
Septal wall of the ventricle	20.5 ± 3.6	23.7 ± 3.8	< 0.01
All locations	22.1 (19.3–24.9)	27.4 (24.2–31.2)	< 0.01
SNR	16.3 (11.8–21.8)	13.7 (9.9–18.4)	0.01
CNR	24.4 (15.5–30.2)	19.2 (14.1–23.2)	< 0.01
Overall quality (scale 1–4)	4.0 (4.0–4.0)	3.0 (3.0–4.0)	< 0.01

SR-DLR, super-resolution deep learning reconstruction; MBIR, model-based iterative reconstruction; SNR, signal-to-noise ratio; CNR, contrast-to-noise ratio

Results

Table 1 lists the baseline clinical characteristics of 70 patients (median age, 69 (IQR, 59–75) years; 50 men). Fifteen patients had prior stent placement (a total of 20 stents). The median body mass index of patients was 24 (IQR, 22–26) kg/m²; their median heart rate during scanning was 55 (IQR, 51–61) bpm.

Of the 70 patients, 63 underwent imaging with prospective ECG gating, and the other seven were imaged with retrospective gating due to arrhythmia or insufficient breath-hold. In patients without stents, the median

Table 3 Characteristics of coronary artery stenosis and stent

Stenosis assessment (n = 210)	
<25%, n (%)	75 (36)
25–49%, n (%)	82 (39)
50–69%, n (%)	36 (17)
70–99%, n (%)	17 (8)
Stent diameter (n = 20)	
2.25 mm, n (%)	1 (5)
2.5 mm, n (%)	7 (35)
2.75 mm, n (%)	2 (10)
3.0 mm, n (%)	7 (35)
3.5 mm, n (%)	2 (10)
4.0 mm, n (%)	1 (5)
Stent length (n = 20)	
	27 ± 11
Stent lesion (n = 20)	
Right coronary artery, n (%)	3 (15)
Left anterior descending artery, n (%)	12 (60)
Left circumflex artery, n (%)	5 (25)

calcium score was 16 (IQR, 0–180). The median effective radiation dose was 0.9 (IQR, 0.6–1.6) mSv.

Comparison of SR-DLR and MBIR

Table 2 displays the reconstruction time, image noise, SNR, CNR, and visual evaluation of the coronary arteries between SR-DLR and MBIR. The reconstruction time was significantly shorter on SR-DLR than on MBIR (median, 97 s; IQR, 88–109 s vs. 173 s; IQR, 164–187 s, p<0.01). The image noise was significantly lower on SR-DLR than that on MBIR (median 22.1 HU; IQR, 19.3–24.9 HU vs. 27.4 HU; IQR, 24.2–31.2 HU, p<0.01). The SNR (median 16.3; IQR, 11.8–21.8 vs. 13.7; IQR, 9.9–18.4 HU, p=0.01) and CNR (median 24.4; IQR, 15.5–30.2 vs. 19.2; IQR, 14.1–23.2, p<0.01) on SR-DLR was significantly higher than those on MBIR. The image quality score on SR-DLR was significantly higher than those on MBIR (median 4.0; IQR, 4.0–4.0 vs. 3.0; IQR, 3.0–4.0, p<0.01).

In both two-volume datasets, a total of 210 major coronary branches were evaluated (Table 3), and representative cases are shown in Figs. 3 and 4. Severe stenosis in the proximal section of the left anterior descending artery was more sharply delineated on SR-DLR than on MBIR, as confirmed by invasive coronary angiography. In contrast, the image quality was lower on SR-DLR images than those on MBIR in patients weighing 144 kg with a body mass index of 46 kg/m² even with higher SNR and CNR on SR-DLR images (Fig. 5). A substantial interobserver agreement was observed on the overall image quality (κ=0.83).

Coronary stent analysis

In 20 stents from fifteen patients, stent assessability was compared between SR-DLR and MBIR (Table 3; Fig. 6). On SR-DLR, stent assessability was 100% (1, 7, 2, 7, 2,

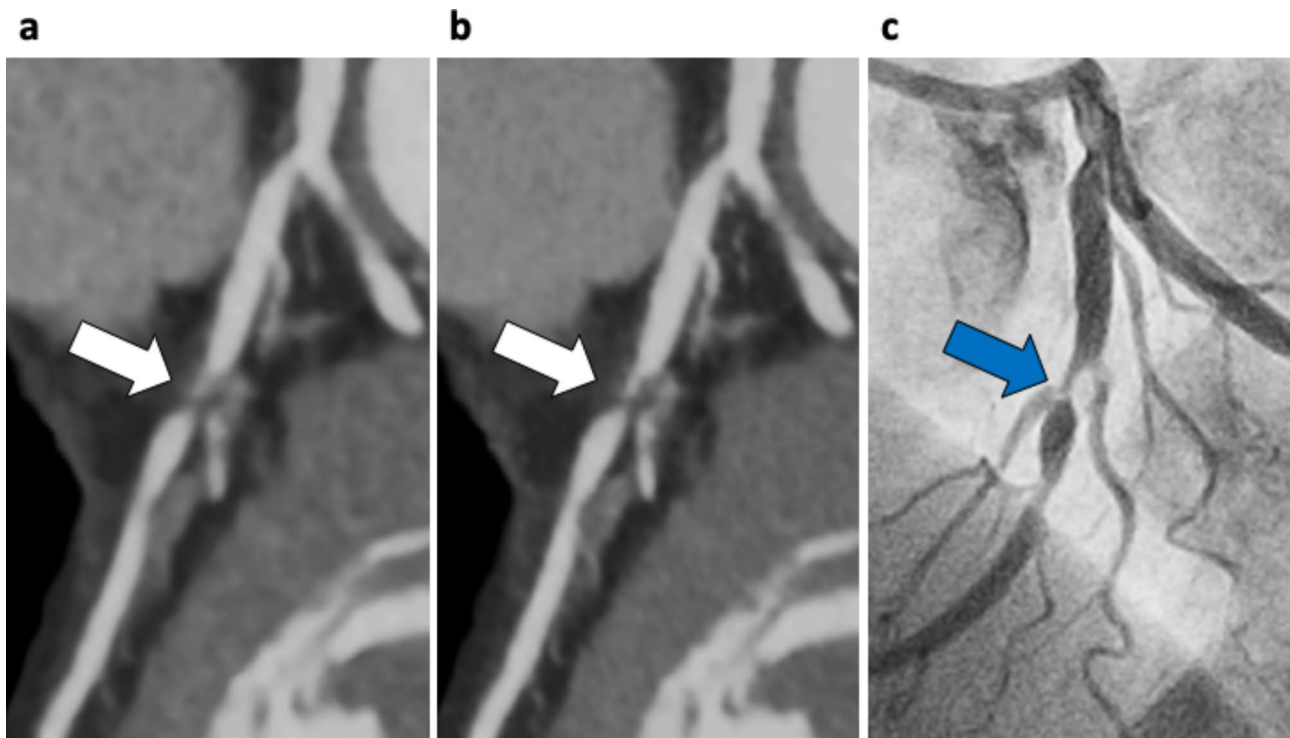


Fig. 3 Case example of a 66-year-old woman with effort angina. Curved planar reformation of the left anterior descending artery (LAD) on MBIR (a) and SR-DLR (b). Severe stenosis in the proximal section of the LAD was more sharply delineated on SR-DLR than those on MBIR (white arrows), which was confirmed using invasive coronary angiography (c, blue arrow). SR-DLR, super-resolution deep learning reconstruction; MBIR, model-based iterative reconstruction; LAD, left anterior descending artery

and 1 of 2.25, 2.5, 2.75, 3.0, 3.5, and 4.0 mm stents). On MBIR, 2.25 mm stents and 3/7 of the 2.5 mm stents cannot be assessed, and the remaining sixteen stents can be assessed (four stents unassessable on MBIR could be assessed on SR-DLR). All twelve stents with a diameter greater than 2.75 mm were assessable both on SR-DLR and MBIR. On quantitative analysis, 60 axial slices of 20 stents were evaluated. The FWHM-stent on SR-DLR was significantly thinner than on MBIR (median, 0.68 mm; IQR, 0.61–0.78 mm vs. 0.81 mm; IQR, 0.72–0.96 mm, $p < 0.01$; Fig. 2e). The FWHM-lumen calculated on SR-DLR was significantly larger than on MBIR (median, 1.84 mm; IQR, 1.65–2.26 mm vs. 1.52 mm; IQR, 1.28–2.25 mm, $p < 0.01$; Fig. 2f).

Discussion

To the best of our knowledge, this is the first study to evaluate the SR-DLR on the image quality of the coronary arteries and in-stent lumen. The image noise was significantly lower, and the SNR and CNR at the proximal coronary arteries was significantly higher on SR-DLR than those on MBIR images. Thus, the overall image quality was significantly better on SR-DLR images. Furthermore, stent struts were significantly thinner, and in-stent lumens were significantly larger on SR-DLR than on MBIR in coronary stent analysis.

Development of CCTA

CCTA has become a first-line test to evaluate patients suspected of coronary artery disease. Nevertheless, some factors such as high image noise, insufficient vessel enhancement, and blooming- and beam-hardening artifacts may hamper the precise evaluation of vessel stenosis and stents [1–3]. Recent developments of UHRCT have enabled the evaluation of calcified, stented, or small diameter segments due to the greater spatial resolution [4–6]. UHR of CCTA with dual-source photon-counting detector CT have also enabled the visualization of calcified plaques with an excellent spatial resolution [20]. However, radiation exposure for UHRCT was higher than that for conventional CCTA [5]. Moreover, UHRCT cannot be used in patients with higher heart rates and weight and those with arrhythmia due to the limitation of the gantry rotation time [4–6]. Remarkably, the whole heart coverage by the area detector with a faster rotation speed contributed to the improvement in the temporal resolution and decreased the radiation exposure and contrast media.

SR-DLR performance

Recently, DLR was developed to improve spatial resolution and low-contrast detectability while reducing noise due to the power of machine learning, a form of artificial intelligence [16]. Especially, SR-DLR algorithm trained using data

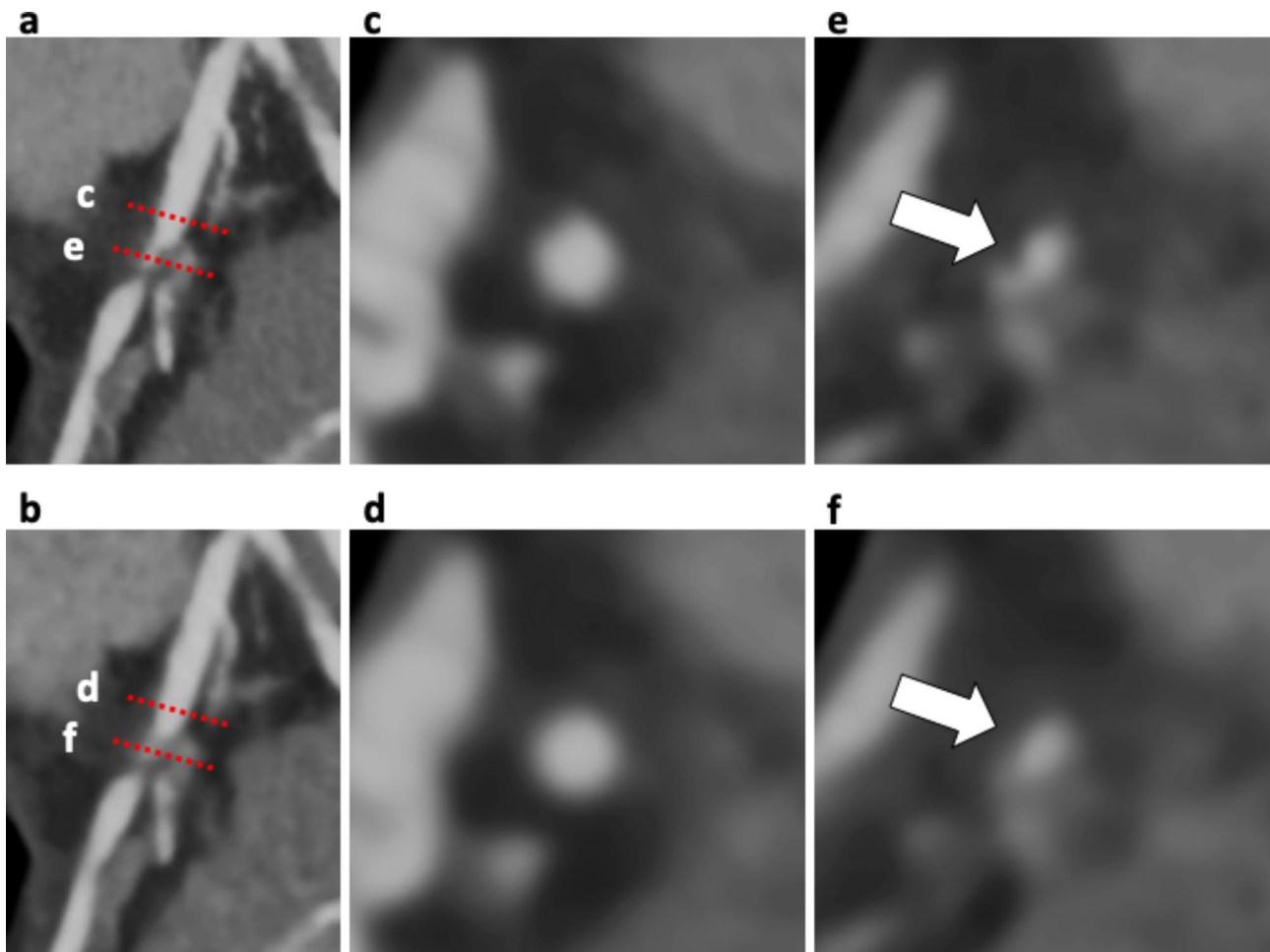


Fig. 4 Case example of the patient in Fig. 2. Curved planar reformation (CPR) images in the proximal section of the left anterior descending artery (LAD) with SR-DLR (**a**) and MBIR (**b**). Two cross-sectional images show the proximal reference site (**c** and **d**) and the site of maximal stenosis (**e** and **f**) correspond to red dashed lines on the CPR image. Coronary lumen and plaque (white arrows) were more sharply delineated on SR-DLR (**c**, **e**) than those on MBIR (**d**, **f**). CPR, curved planar reformation; LAD, left anterior descending artery; SR-DLR, super-resolution deep learning reconstruction; MBIR, model-based iterative reconstruction

acquired on the commercially available UHRCT system is available [7, 8]. SR-DLR algorithm features UHR 0.25 mm detectors to maximize the inherent spatial resolution on the conventional 320-detector row CT. With conventional reconstruction, a long tradeoff between spatial resolution and noise has forced CT systems to operate at much lower spatial resolution levels than the detector and focal spots are capable of producing maintenance at clinically acceptable dose levels. With DLR, not only can this resolution be utilized, without increasing the dose or noise, but it also can be enhanced further. Furthermore, the neural network behind SR-DLR does not learn features solely in the axial plane but rather in three dimensions, indicating that signal features are identified and preserved in all three planes. Therefore, SR-DLR is found to be well-suited for cardiac exams, which are usually reviewed in CPR.

In several studies, the spatial resolution is reported be higher on MBIR than on filtered back projection and

hybrid-IR images [21, 22]. Reportedly, the sophisticated MBIR modeling reduces blooming artifacts and yields a better image quality than hybrid IR [23]. Recently, several studies have reported that the image noise was lower and the coronary artery delineation was better on SR-DLR scans compared with conventional reconstruction techniques such as hybrid-IR, MBIR, and DLR [9, 10]. In this study, SR-DLR images yielded a higher image quality including image noise reduction and better spatial resolution than those on MBIR. Moreover, the reconstruction time was significantly shorter on SR-DLR than on MBIR. Hence, using SR-DLR would improve the utility of CCTA in routine clinical practice.

Assessment of the in-stent lumen on CCTA with SR-DLR

Direct visualization of the in-stent lumen on CCTA was challenging mainly due to beam hardening and partial volume effects. Motoyama et al. have reported that the in-stent

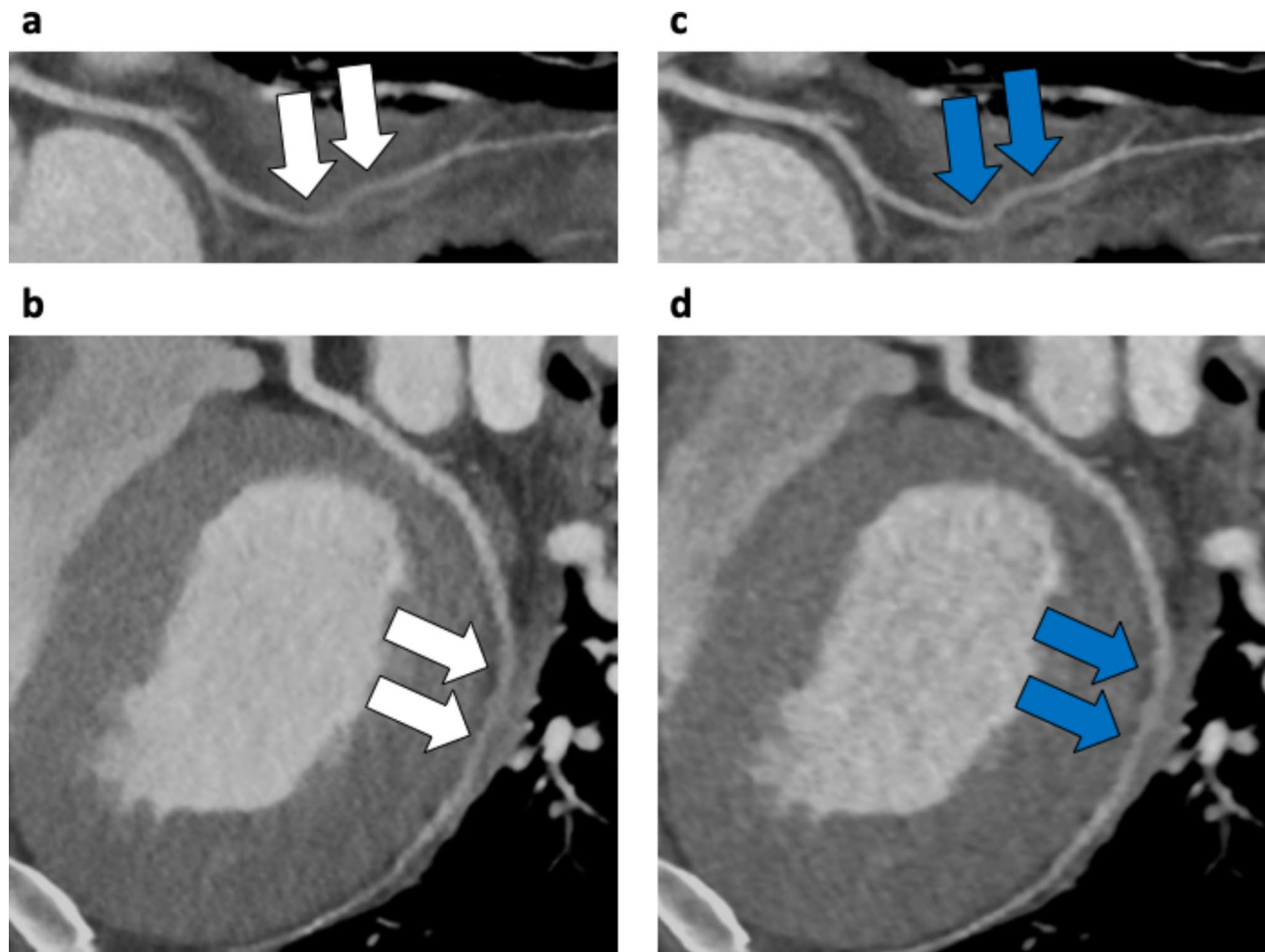


Fig. 5 Case example of a 34-year-old man weighing 144 kg with a body mass index of 46 kg/m². Curved planar reformation of the left circumflex artery taken at 120 kV, 750 mA, with prospective ECG gating. **a, b**: SR-DLR image (signal-to-noise ratio (SNR), 17.4; contrast-to-noise ratio (CNR), 21.0). The image quality was rated as fair with marked noise-related blurring (white arrows). **c, d**: MBIR image (SNR, 16.0; CNR, 17.8). The image quality was rated as good with some noise-related blurring (blue arrows). SR-DLR, super-resolution deep learning reconstruction; SNR, signal-to-noise ratio; CNR, contrast-to-noise ratio; MBIR, model-based iterative reconstruction

lumen of stents with ≥ 2.5 mm diameter could be assessed on UHRCT because of improved spiral resolution [4]. In this study, SR-DLR could evaluate all stents, including 2.25 and 2.5 mm stents. Moreover, SR-DLR demonstrates better strut delineation of the stent and in-stent lumen that are more accurate than MBIR. The edge has been reportedly sharper on MBIR than on images reconstructed with conventional filtered back projection or hybrid IR [23, 24]. SR-DLR had similar effects on the boundary of coronary stents.

In contrast, the image quality of SR-DLR was lower in patients with higher weight. Training the deep learning neural network with educational images from higher weight patients would make the SR-DLR more valuable.

Limitations

First, our study population was small. Second, the diagnostic accuracy of CCTA was confirmed in comparison with invasive coronary angiography in a limited number of

enrolled patients only. Large-scale studies are required to validate and expand our initial experience using invasive coronary angiography as the reference standard. Third, the SNR and CNR were evaluated in the proximal coronary arteries only. The small diameter of distal segments makes it impossible to place ROIs without including parts of the vessel walls and adjacent tissues. Moreover, no stents were evaluated on side-branch in this study. SR-DLR may be able to evaluate side-branch stents as well as small-diameter stents based on the results of this study, but further studies are needed to evaluate side-branch stents. Fourth, the SR-DLR algorithm is currently vendor-specific. Finally, the population of this study is less challenging for CCTA scans. In further studies, the value of SR-DLR needs to be proven in patients with high calcium scores to assess the delineation of the calcified plaques, in patients with high body weight, and in patients with arrhythmias. Comparative studies of coronary stent evaluation, including stents in side-branch,

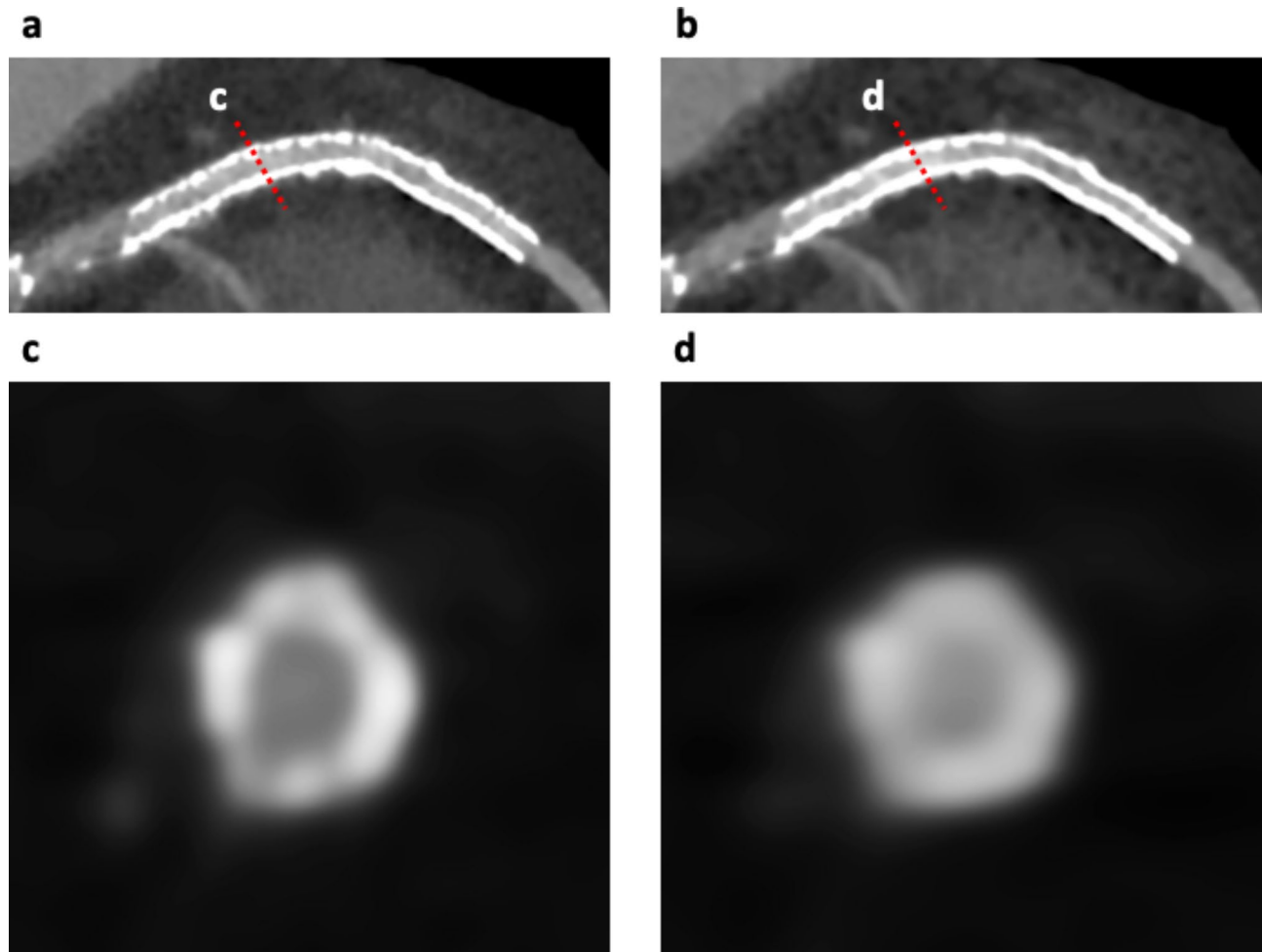


Fig. 6 Case example of an 80-year-old woman with a stent in the left descending coronary artery. Curved planar reformation (CPR) images of the 2.5 mm stent in the left anterior descending artery (LAD) with SR-DLR (a) and MBIR images (b). Cross-sectional images showing the in-stent lumen and stent strut (c and d) corresponding to red dashed lines on the CPR image. In-stent lumen was clearly visualized on SR-DLR (a and c; assessable) compared with MBIR (b and d; unassessable). CPR, curved planar reformation; LAD, left anterior descending artery; SR-DLR, super-resolution deep learning reconstruction; MBIR, model-based iterative reconstruction

between UHRCT and 320-detector row CT scanner with SR-DLR are also required to assess whether SR-DLR can overcome the limitations of UHRCT.

Conclusion

SR-DLR might improve the image quality of the coronary arteries and in-stent lumen at CCTA. Datasets reconstructed with SR-DLR empower the clinician with the high-contrast signal definition and reduce noise, relative to conventional MBIR.

Abbreviations

CCTA	Coronary computed tomography angiography
SR-DLR	Super-resolution deep learning reconstruction
MBIR	Model-based iterative reconstruction
UHRCT	Ultrahigh spatial resolution computed tomography
EKG	Electrocardiogram
DCNN	Deep convolutional neural network
SD	Standard deviation
ROI	Region of interest

SNR	Signal-to-noise ratio
CNR	Contrast-to-noise ratio
CPR	Curved planar reformation
FWHM-lumen	Full width at half maximum of the lumen
FWHM-stent	Full width at half maximum of the stent
IQR	Interquartile range
HR	High resolution
LR	Low resolution
HN	High noise
LN	Low noise

Acknowledgements

The authors would like to thank Enago (www.enago.jp) for the English language review. This work was supported by JSPS KAKENHI Grant Number JP22K07803.

Authors contributions

MO designed and drafted the manuscript. MO and KY acquired data and assessed CCTA. MS and TO supported the statistical analysis. YU, TC, and TS provided technical assistance. KY substantially contributed to the manuscript and revised it critically for important intellectual content. All authors approved the submitted version.

Funding

Not applicable.

Data Availability

The dataset analyzed during the present study is available from the corresponding author on reasonable request.

Declarations

Competing interests

Kunihiro Yoshioka received a research grant from Canon Medical Systems Co. Ltd. Other authors declare that they have no conflict of interest.

Ethics approval and consent to participate

The study was approved by the institution's human research committee (Iwate Medical University). All methods were carried out in accordance with relevant guidelines and regulations, and informed consent was obtained from all individual participants included in the study.

Consent for publication

Not Applicable.

Received: 12 October 2022 / Accepted: 25 October 2023

Published online: 30 October 2023

References

- Raff GL, Gallagher MJ, O'Neill WW, Goldstein JA. Diagnostic accuracy of non-invasive coronary angiography using 64-slice spiral computed tomography. *J Am Coll Cardiol*. 2005;46:552–7. <https://doi.org/10.1016/j.jacc.2005.05.056>.
- Nikolaou K, Knez A, Rist C, Wintersperger BJ, Leber A, Johnson T, Reiser MF, Becker CR. Accuracy of 64-MDCT in the diagnosis of Ischemic Heart Disease. *AJR Am J Roentgenol*. 2006;187:111–7. <https://doi.org/10.2214/AJR.05.1697>.
- Herzog C, Zwerner PL, Doll JR, Nielsen CD, Nguyen SA, Savino G, Vogl TJ, Costello P, Schoepf UJ. Significant coronary artery stenosis: comparison on per-patient and per-vessel or per-segment basis at 64-section CT angiography. *Radiology*. 2007;244:112–20. <https://doi.org/10.1148/radiol.2441060332>.
- Motoyama S, Ito H, Sarai M, Nagahara Y, Miyajima K, Matsumoto R, Doi Y, Kataoka Y, Takahashi H, Ozaki Y, Toyama H, Katada K. Ultra-high-resolution computed tomography angiography for assessment of coronary artery stenosis. *Circ J*. 2018;82:1844–51. <https://doi.org/10.1253/circj.CJ-17-1281>.
- Takagi H, Tanaka R, Nagata K, Ninomiya R, Arakita K, Schuijff JD, Yoshioka K. Diagnostic performance of coronary CT angiography with ultra-high-resolution CT: comparison with invasive coronary angiography. *Eur J Radiol*. 2018;101:30–7. <https://doi.org/10.1016/j.ejrad.2018.01.030>.
- Latina J, Shabani M, Kapoor K, Whelton SP, Trost JC, Sesso J, Demehri S, Mahesh M, Lima JAC, Arbab-Zadeh A. Ultra-high-resolution coronary CT angiography for assessment of patients with severe coronary artery calcification: initial experience. *Radiol Cardiothorac Imaging*. 2021;3:e210053. <https://doi.org/10.1148/ryct.2021210053>.
- Hernandez AM, Shin DW, Abbey CK, Seibert JA, Akino N, Goto T, Vaishnav JY, Boedeker KL, Boone JM. Validation of synthesized normal-resolution image data generated from high-resolution acquisitions on a commercial CT scanner. *Med Phys*. 2020;47:4775–85. <https://doi.org/10.1002/mp.14395>.
- Lee T, Zhou J, Schuzer J, Matsuura M, Nemoto T, Taguchi H, Yu Z, Cai L. Deep learning enabled wide-coverage high-resolution cardiac CT. *SPIE Med Imaging*. 2022. <https://doi.org/10.1117/12.2611817>. San Diego, California, United States.
- Tatsugami F, Higaki T, Kawashita I, Fukumoto W, Nakamura Y, Matsuura M, Lee TC, Zhou J, Cai L, Kitagawa T, Nakano Y, Awai K. Improvement of spatial resolution on coronary CT angiography by using Super-resolution Deep Learning Reconstruction. *Acad Radiol*. 2023 Jan 19;S1076-6332(22)00700-0. <https://doi.org/10.1016/j.acra.2022.12.044>.
- Sato H, Fujimoto S, Tomizawa N, Inage H, Yokota T, Kudo H, Fan R, Kawamoto K, Honda Y, Kobayashi T, Minamino T, Kogure Y. Impact of a deep learning-based Super-resolution Image Reconstruction technique on high-contrast computed tomography: a Phantom Study. *Acad Radiol*. 2023 Jan 21;S1076-6332(22)00696-1. <https://doi.org/10.1016/j.acra.2022.12.040>.
- Abbara S, Arbab-Zadeh A, Callister TQ, Desai MY, Mamuya W, Thomson L, Weigold WG. SCCT guidelines for performance of coronary computed tomographic angiography: a report of the Society of Cardiovascular Computed Tomography Guidelines Committee. *J Cardiovasc Comput Tomogr*. 2009;3:190–204. <https://doi.org/10.1016/j.jcct.2009.03.004>.
- Abbara S, Blanke P, Maroules CD, Cheezum M, Choi AD, Han BK, Marwan M, Naoum C, Norgaard BL, Rubinshtein R, Schoenhagen P, Villines T, Leipsic J. SCCT guidelines for the performance and acquisition of coronary computed tomographic angiography: a report of the society of cardiovascular computed tomography Guidelines Committee: endorsed by the North American Society for Cardiovascular Imaging (NASCI). *J Cardiovasc Comput Tomogr*. 2016;10:435–49. <https://doi.org/10.1016/j.jcct.2016.10.002>.
- The 2007 recommendations of the International Commission on Radiological Protection. *Ann ICRP ICRP Publication*. 2007;37:1–332. <https://doi.org/10.1016/j.icrp.2007.10.003>. ICRP publication 103.
- Boedeker K. AiCE Deep Learning Reconstruction: bringing the power of Ultra-high Resolution CT to routine imaging, technical white paper. Canon Medical Systems Corporation; 2018.
- Leipsic J, Abbara S, Achenbach S, Cury R, Earls JP, Mancini GJ, Nieman K, Pontone G, Raff GL. SCCT guidelines for the interpretation and reporting of coronary CT angiography: a report of the Society of Cardiovascular Computed Tomography Guidelines Committee. *J Cardiovasc Comput Tomogr*. 2014;8:342–58. <https://doi.org/10.1016/j.jcct.2014.07.003>.
- Tatsugami F, Higaki T, Nakamura Y, Yu Z, Zhou J, Lu Y, Fujioka C, Kitagawa T, Kihara Y, Iida M, Awai K. Deep learning-based image restoration algorithm for coronary CT angiography. *Eur Radiol*. 2019;29:5322–9. <https://doi.org/10.1007/s00330-019-06183-y>.
- Lembcke A, Wiese TH, Schnorr J, Wagner S, Mews J, Kroencke TJ, Enzweiler CN, Hamm B, Taupitz M. Image quality of noninvasive coronary angiography using multislice spiral computed tomography and electron-beam computed tomography: intraindividual comparison in an animal model. *Invest Radiol*. 2004;39:357–64. <https://doi.org/10.1097/01.rii.0000123316.10765.6c>.
- Tatsugami F, Husmann L, Herzog BA, Burkhard N, Valenta I, Gaemperli O, Kaufmann PA. Evaluation of a body mass index-adapted protocol for low-dose 64-MDCT coronary angiography with prospective ECG triggering. *AJR Am J Roentgenol*. 2009;192:635–8. <https://doi.org/10.2214/AJR.08.1390>.
- Groen JM, Greuter MJ, van Ooijen PM, Oudkerk M. A new approach to the assessment of lumen visibility of coronary artery stent at various heart rates using 64-slice MDCT. *Eur Radiol*. 2007;17:1879–84. <https://doi.org/10.1007/s00330-006-0568-8>.
- Mergen V, Sartoretti T, Baer-Beck M, Schmidt B, Petersilka M, Wildberger JE, Euler A, Eberhard M, Alkadhi H. Ultra-high-resolution Coronary CT Angiography with Photon-counting detector CT: feasibility and image characterization. *Invest Radiol*. 2022;57(12):780–8. <https://doi.org/10.1097/RLI.0000000000000897>.
- Nelson RC, Feuerlein S, Boll DT. New iterative reconstruction techniques for cardiovascular computed tomography: how do they work, and what are the advantages and disadvantages? *J Cardiovasc Comput Tomogr*. 2011;5:286–92. <https://doi.org/10.1016/j.jcct.2011.07.001>.
- Geyer LL, Schoepf UJ, Meinel FG, Nance JW Jr, Bastarrika G, Leipsic JA, Paul NS, Rengo M, Laghi A, De Cecco CN. State of the art: iterative CT reconstruction techniques. *Radiology*. 2015;276:339–57. <https://doi.org/10.1148/radiol.2015132766>.
- Tatsugami F, Higaki T, Sakane H, Fukumoto W, Kaichi Y, Iida M, Baba Y, Kiguchi M, Kihara Y, Tsushima S, Awai K. Coronary artery stent evaluation with model-based iterative reconstruction at coronary CT angiography. *Acad Radiol*. 2017;24:975–81. <https://doi.org/10.1016/j.acra.2016.12.020>.
- Yokomachi K, Tatsugami F, Higaki T, Kume S, Sakamoto S, Okazaki T, Kurisu K, Nakamura Y, Baba Y, Iida M, Awai K. Neointimal formation after carotid artery stenting: phantom and clinical evaluation of model-based iterative reconstruction (MBIR). *Eur Radiol*. 2019;29:161–7. <https://doi.org/10.1007/s00330-018-5598-5>.

Publisher's Note

Springer Nature remains neutral with regard to jurisdictional claims in published maps and institutional affiliations.